Supporting information for

A coumarin-based fluorescent probe for monitoring labile ferrous iron in living system

Lingliang Long,[a,*] Ning Wang,[a] Yuanyuan Han,[a] Meiyu Huang,[a] Xiangqi Yuan,[a] Siyu Cao,[a] Aihua Gong,[b,*] and Kun Wang [a,*]

[a] School of Chemistry and Chemical Engineering, Jiangsu University, Zhenjiang, Jiangsu 212013 (P. R. China).
[b] School of Medicine, Jiangsu University, Zhenjiang, Jiangsu 212013 (P. R. China).

Email: longlingliang@ujs.edu.cn; ahg5@ujs.edu.cn; wangkun@ujs.edu.cn.

Table of contents

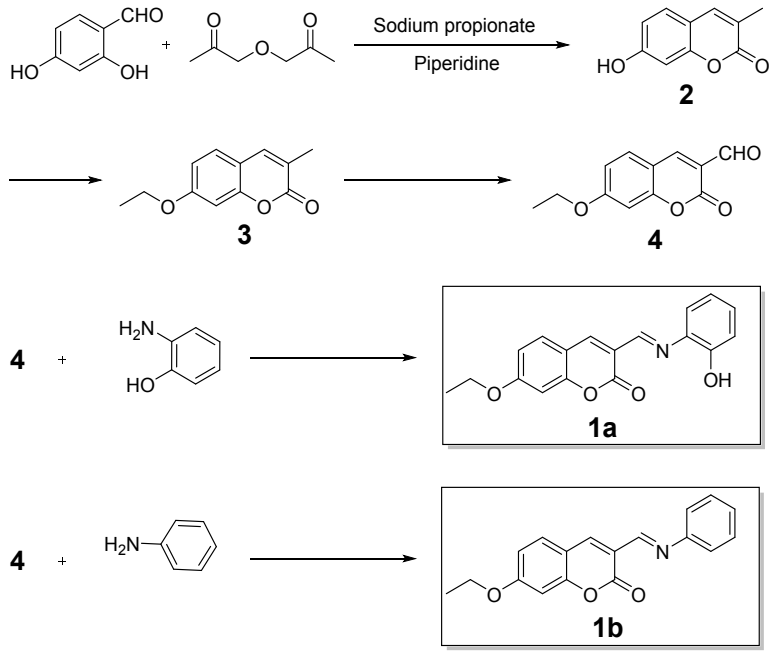

Scheme S1. The synthetic procedure of compounds **1a** and **1b**.

Preparation of the test solution

The stock solution of probe **1a** (1×10^{-4} M) was prepared in DMF, and the stock solution of various relevant metal ions (1×10^{-3} M) was prepared by dissolving an appropriate amount of metal ions in water. The test solution of the probe **1a** (10 μM) in 20 mM potassium phosphate buffer/DMF (pH 7.4, 1:1 v/v) was prepared by placing 0.5 mL of the probe **1a** stock solution, 2.0 mL DMF and an appropriate aliquot of each testing species stock into a 5.0 mL volumetric flask, and then diluting the solution to 5 mL with 20 mM potassium phosphate buffer (pH 7.4). The resulting solution was shaken well and incubated at room temperature for 2 min before recording the spectra.

Determination of fluorescence quantum yield

Fluorescence quantum yield was determined using the solutions of quinine sulfate (Φ_F = 0.546 in 1N H_2SO_4)[1] as a standard. The quantum yield was calculated using the following equation:[2-4]

$$\Phi_{F(X)} = \Phi_{F(S)} (A_S F_X / A_X F_S) (n_X / n_S)^2$$

Where Φ_F is the fluorescence quantum yield, A is the absorbance at the excitation wavelength, F is the area under the corrected emission curve, and n is the refractive index of the solvents used. Subscripts S and X refer to the standard and to the unknown, respectively.

Determination of the detection limit

The detection limit was determined from fluorescence titration data based on a reported method.[5-9] According to the result of titration experiment, the graph of $(F_{min}-F) / (F_{min}-F_{max})$ versus log $[Fe^{2+}]$ was plotted, where the F is the fluorescence intensity at 452 nm, F_{min} and F_{max} are the minimum and maximum fluorescence intensity at 452 nm respectively. A linear regression curve was then fitted (Figure S5), and the intercept of

the line at x-axis was taken as detection limit.

Computational details

The UV/Vis absorption and the emission properties of probe **1a** and compound **5** were studied with DFT/TDDFT calculations at the B3LYP/6-31G(d,p)/level using Gaussian 09.[10] Water was used as the solvent in the calculations (PCM model). First, the optimized ground-state geometries of probe **1a** and compound **5** were obtained. The UV/Vis absorption was calculated by the TDDFT method based on the ground-state geometry (vertical excitation, Franck-Condon principle). The geometry of excited state was optimized and the emission was calculated with the TDDFT method (usually excited state is responsible for the fluorescence, Kasha's role). The vertical excitation and the emission related calculations were based on the optimized excited state.

The geometry optimization for **1a**-Fe^{2+} complexes was carried out in vacuum using B3LYP potential in conjuration with a 6-31G(d,p) basis set for the H, C, N, and O atoms, and a LANL2DZ effective core potential (ECP) basis set for the Fe atom, as implemented in GAUSSIAN 09 software package. This level is often estimated to be adequate for the geometry optimization of aromatic compounds with metal interactions. Harmonic vibrations were also calculated for the obtained structure to establish that a true minimum was reached.

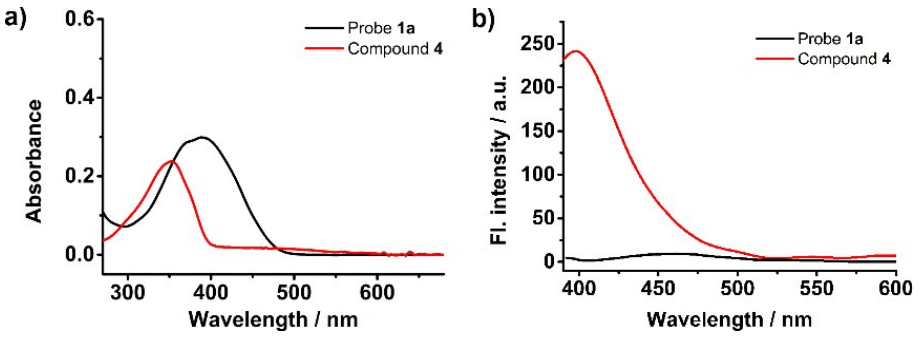

Figure S1. The UV/Vis absorption spectra (a) and fluorescence emission spectra (b) of probe **1a** and compound **4** in 20 mM potassium phosphate buffer/DMF (1:1 v/v, pH 7.4). The excitation wavelengths for **1a** and **4** were 390nm and 350nm, respectively.

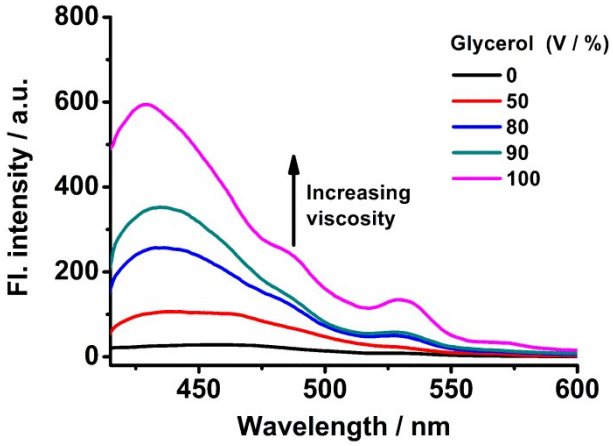

Figure S2. Fluorescence emission spectra of probe **1a** (10 μM) in the glycerol / DMF solution with increasing viscosity (λ_{ex} = 390 nm).

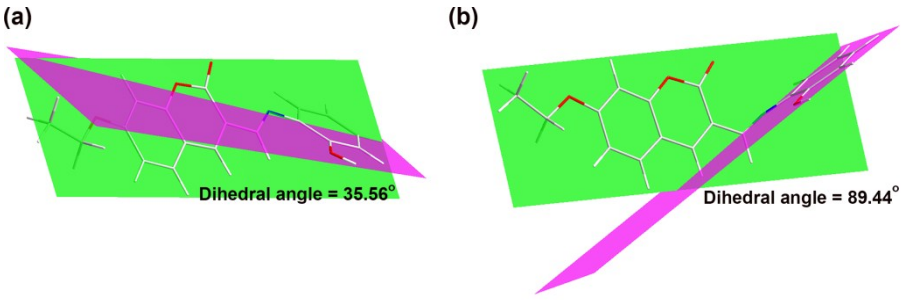

Figure S3. The dihedral angles of probe **1a** between the coumarin ring and the phenol ring in (a) ground state geometry and (b) first excited singlet state geometry.

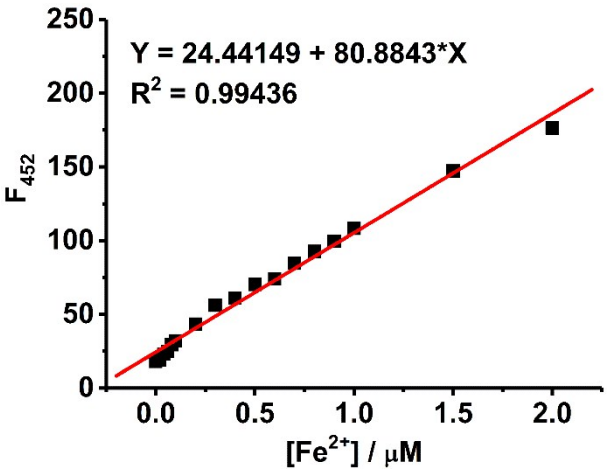

Figure S4. The linear relationship of fluorescence intensity (F_{452}) to various amount of Fe^{2+} (0 to 2 μM).

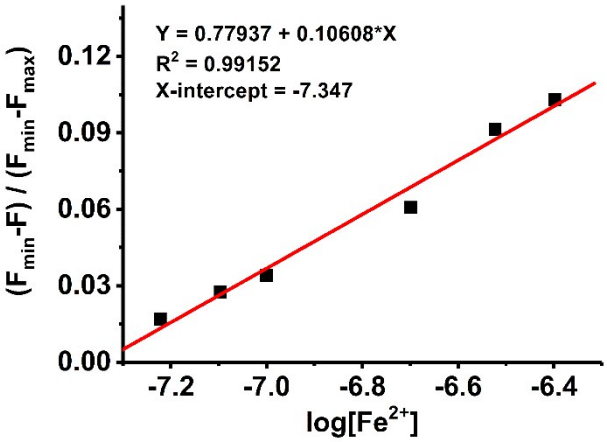

Figure S5. Plot of $(F_{min}- F) / (F_{min}-F_{max})$ versus log $[Fe^{2+}]$ for probe **1a**. Calculated detection limit = 45 nM.

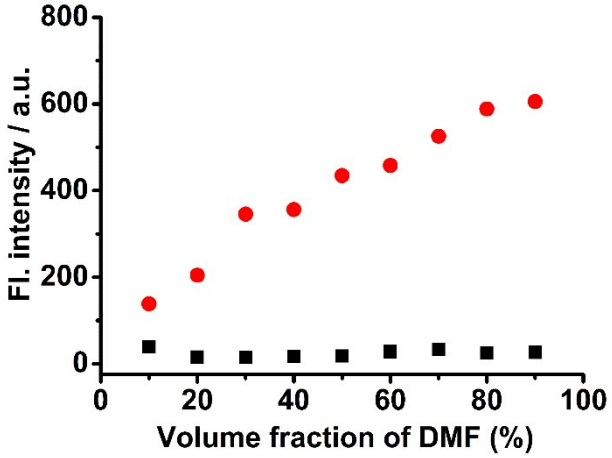

Figure S6. Variations in the fluorescence intensity (I_{452}) of probe **1a** (10 μM) recorded in the presence (●) or absence (■) of Fe^{2+} (20 μM) as a function of the volume fraction of DMF. The excitation wavelength was 390 nm.

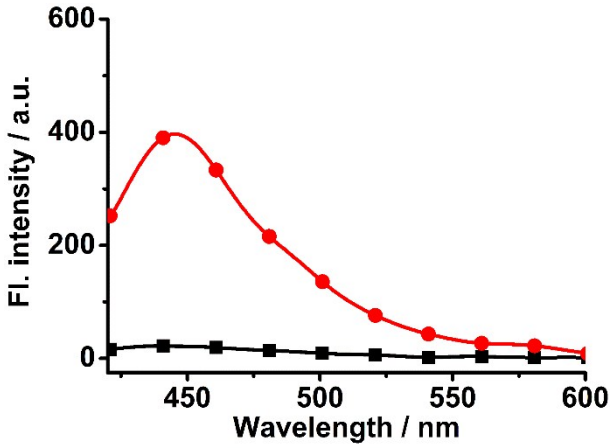

Figure S7. The fluorescence emission spectra of probe **1a** (10 μM) in the absence (■) and presence (●) of Fe^{2+} (20 μM) in 20 mM potassium phosphate buffer (pH 7.4) with ethanol as co-solvent (50%).

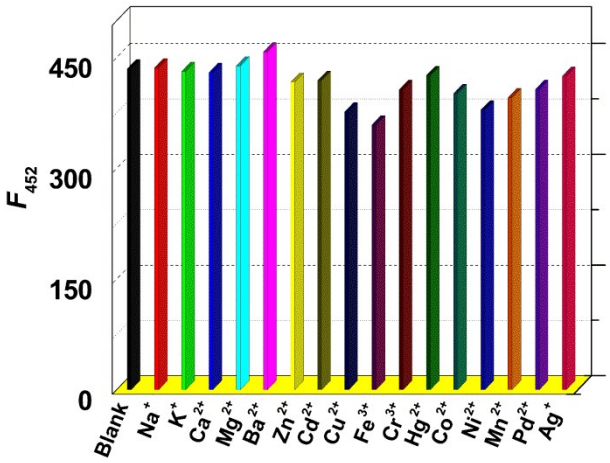

Figure S8. Fluorescence response of probe **1a** (10 μM) to 20 μM of Fe^{2+} in the presence of 20 μM of other metal ions. The excitation wavelength was 390 nm.

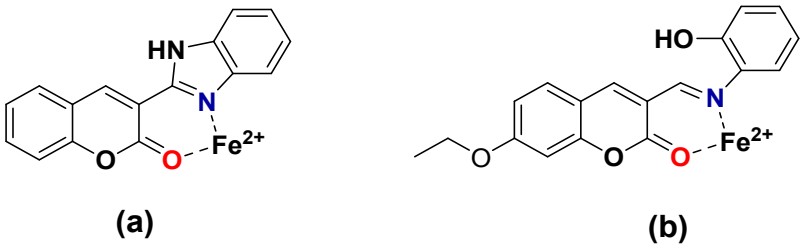

Figure S9. (a) The binding of 2-coumarinylbenzimidazole with Fe^{2+} and (b) the proposed binding of probe **1a** with Fe^{2+}.

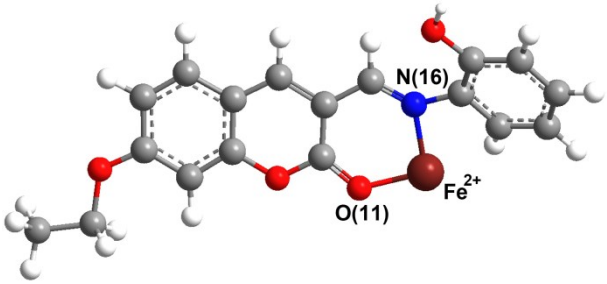

Figure S10. Calculated energy-minimized structure of probe **1a** with Fe^{2+}.

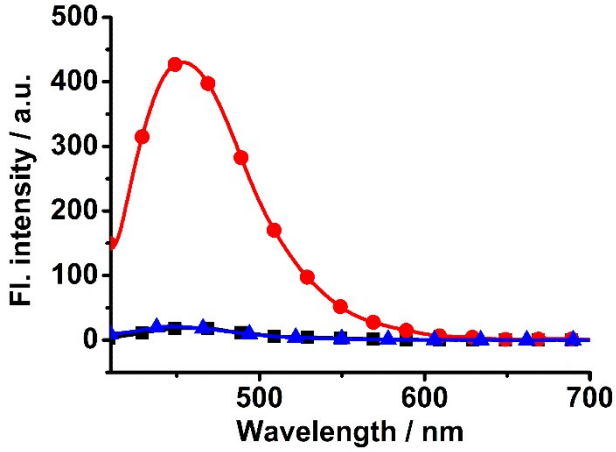

Figure S11 The fluorescence emission spectra of probe **1a** (10 μM) incubated in 20 mM potassium phosphate buffer/DMF (1:1 v/v, pH 7.4) solutions for 2 min (■) and 5 hours (▲). For comparison, the fluorescence emission spectra of probe **1a** (10 μM) with Fe^{2+} (20 μM) for 2 min was also shown (●). The excitation wavelength was 390 nm.

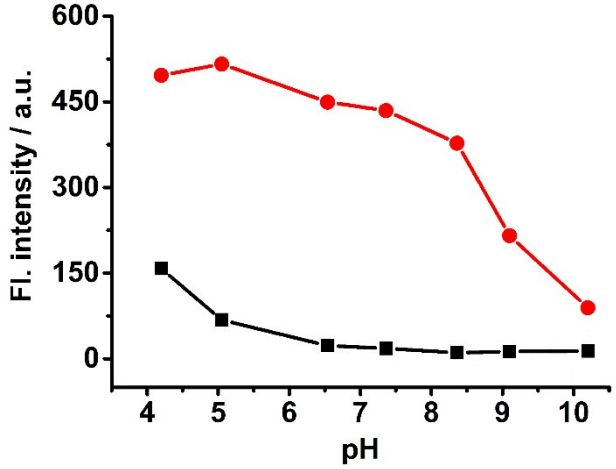

Figure S12. The variations of fluorescence intensity (F_{452}) of probe **1a** (10 μM) in the presence (●) or absence (■) of Fe^{2+} (20 μM) as a function of pH. Excitation wavelength was 390 nm.

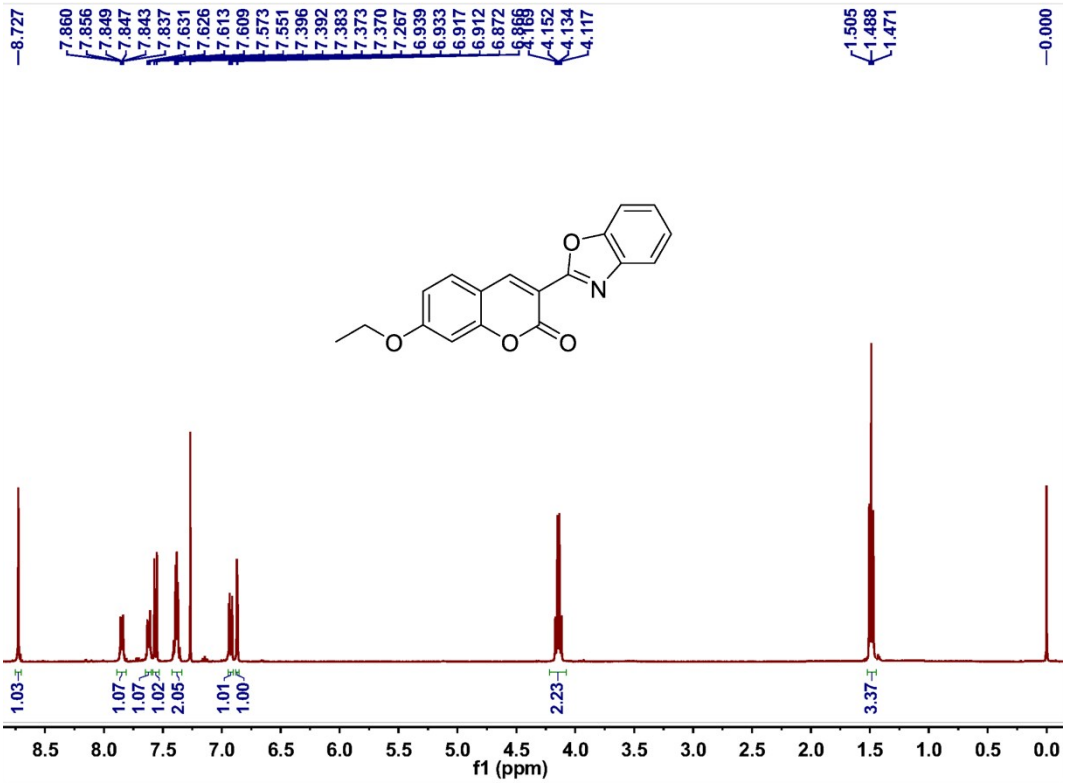

Figure S13. The ^{1}H NMR spectra of the isolated product of probe **1a** with Fe^{2+}.

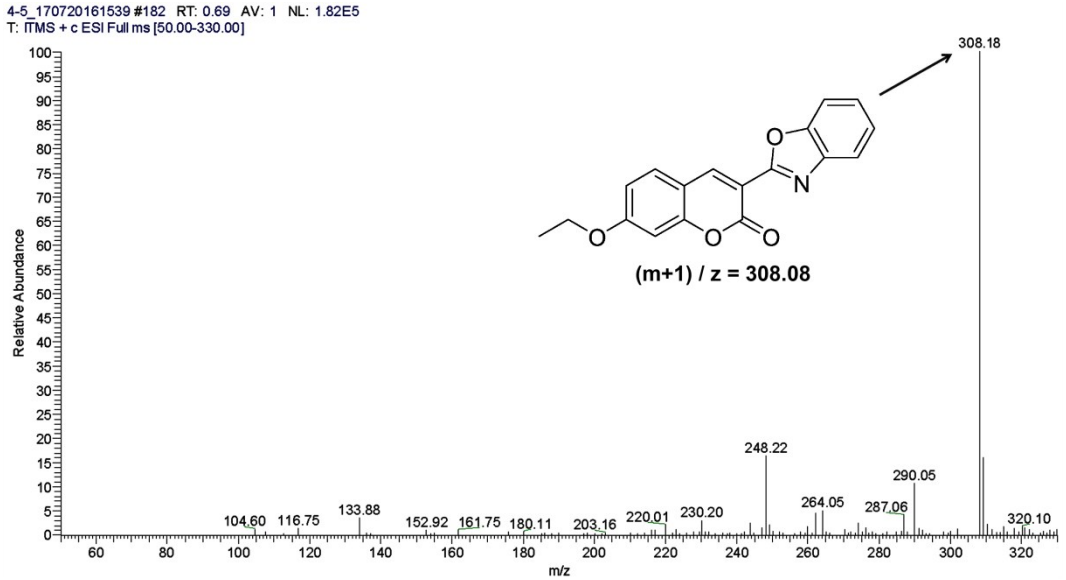

Figure S14. The ESI-Ms spectra of the isolated product of probe **1a** with Fe^{2+}.

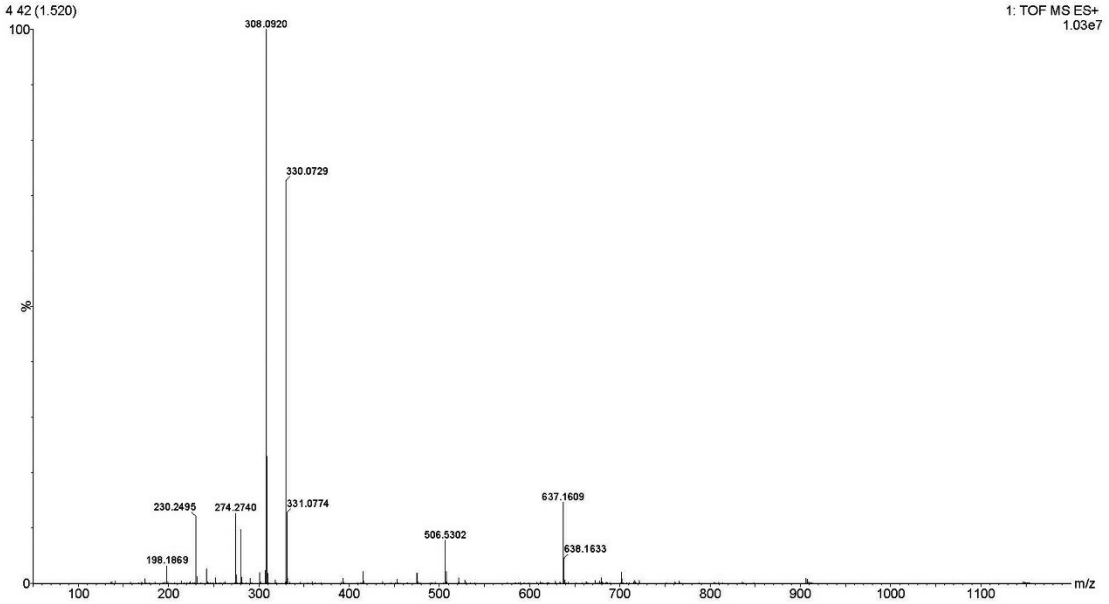

Figure S15. The high-resolution mass spectrometry (HRMS) of the isolated product of probe **1a** with Fe^{2+} (compound **5**). HRMS Calcd for $C_{18}H_{14}NO_4^+$ $[M+H]^+$: 308.0917; found: 308.0920.

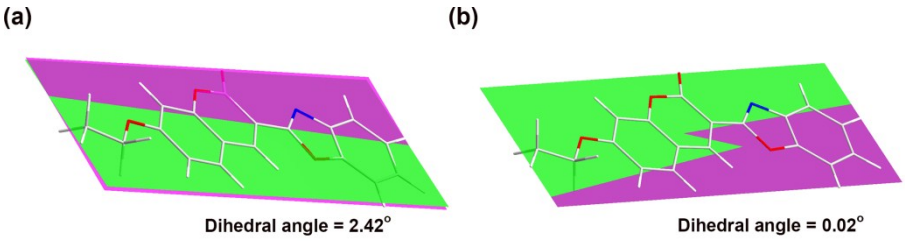

Figure S16. The dihedral angles of compound **5** between the coumarin ring and the benzoxazole ring in (a) ground state geometry and (b) first excited singlet state geometry.

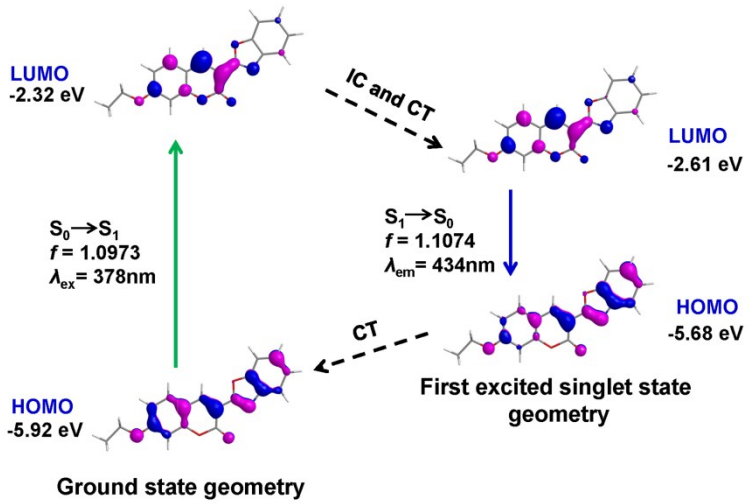

Figure S17. Rationalization of the UV/Vis absorption and the strong fluorescence of compound **5**: the geometry relaxation upon photoexcitation and the frontier molecular orbitals (MOs) involved in the vertical excitation (i.e., UV/Vis absorption, the left columns) and emission (the right column) of compound **5**. The vertical excitations were calculated based on the optimized ground state geometry, the emission was calculated based on the optimized geometry of the excited state. Water was used as the solvent (PCM model). IC stands for internal conversion and CT stands for conformation transformation. Excitation and radiative processes are marked as solid arrow and the non-radiative processes are marked by dotted arrow.

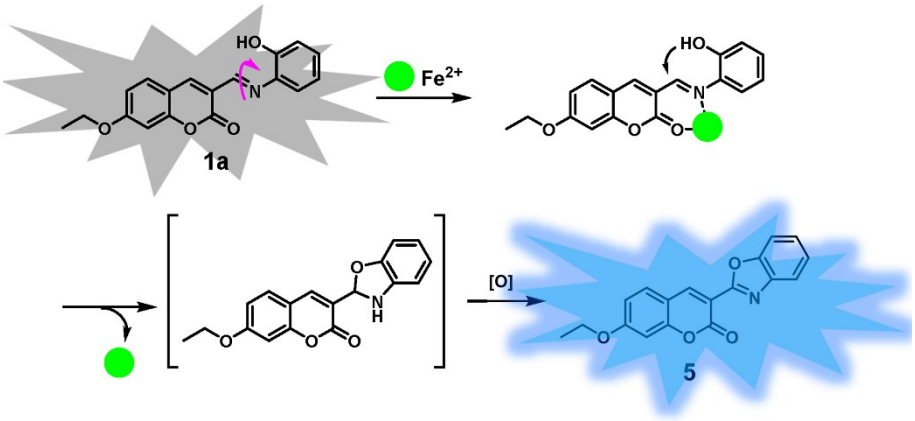

Scheme S2. A plausible reaction mechanism of probe **1a** with Fe^{2+}.

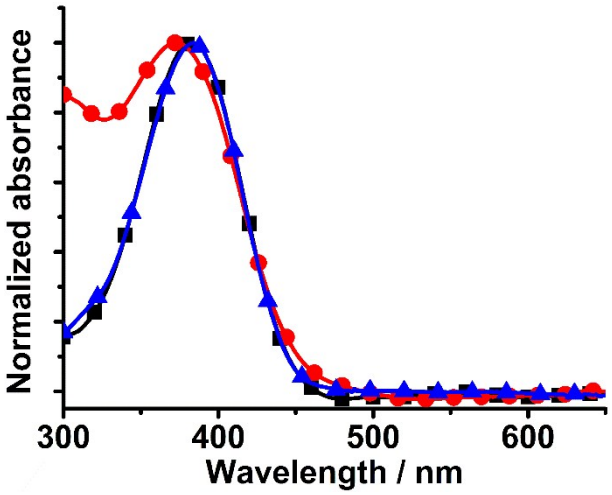

Figure S18. The normalized UV/Vis absorption spectra of **1b** (■), **1b** + Fe^{2+} (●), and the above **1b** + Fe^{2+} solution after removing Fe^{2+} (▲). The Fe^{2+} in the **1b** + Fe^{2+} solution was removed according to the following procedures: the NaOH solution was added to the solution of **1b** + Fe^{2+}, and the resulting precipitation was removed by filtration. The filtrate was neutralized by addition of hydrochloric acid. Then the obtained solution was utilized for UV/Vis absorption spectra test.

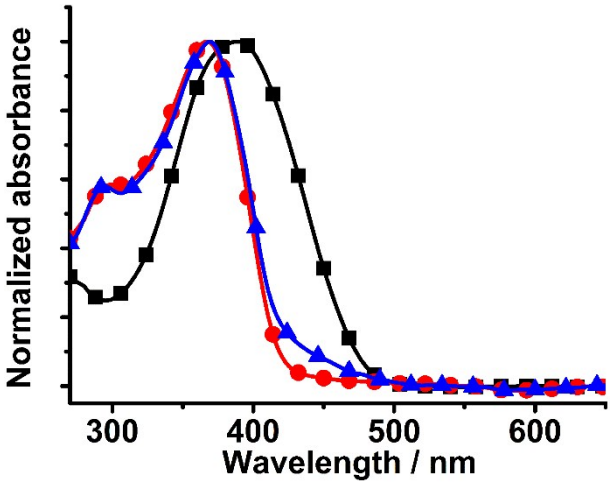

Figure S19. The normalized UV/Vis absorption spectra of **1a** (■), **1a** + Fe^{2+} (●), and the above **1a** + Fe^{2+} solution after removing Fe^{2+} (▲). The Fe^{2+} in the **1a** + Fe^{2+} solution was removed according to a similar procedure in Figure S14.

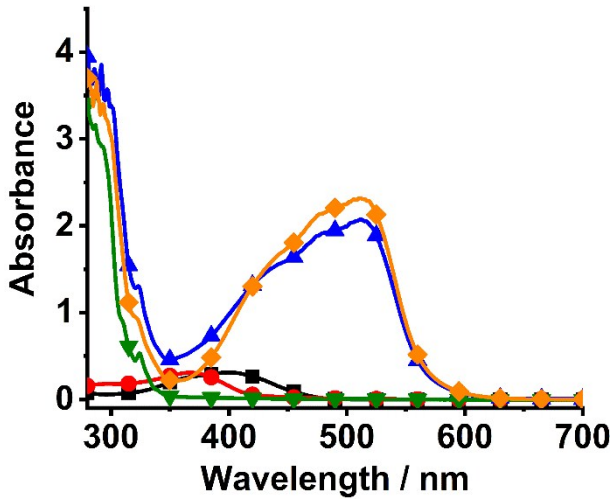

Figure S20. The UV/Vis absorption spectra of **1a** (10 μM) (■); **1a** (10 μM) and Fe^{2+} (20 μM) incubated for 2 min (●); **1a** (10 μM) and Fe^{2+} (20 μM) incubated for 2 min, then further treated with 1,10-phenanthroline (60 μM) (▲). For comparison, the UV/Vis absorption spectra of 1,10-phenanthroline (60 μM) (▼), 1,10-phenanthroline (60 μM) with Fe^{2+} (20 μM) (◆) were also displayed.

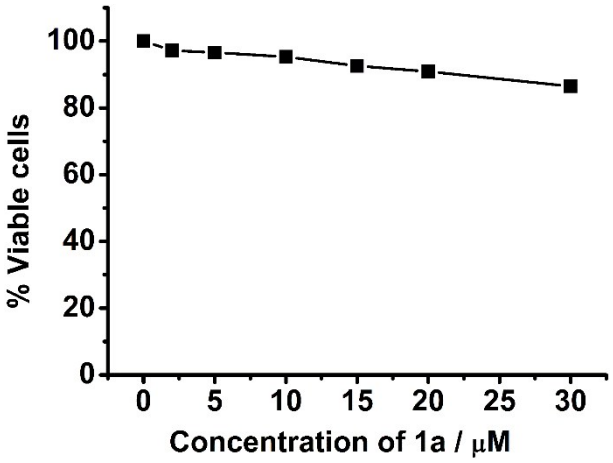

Figure S21. Cytotoxicity of probe **1a** in cultured HepG2 cells. The cells were incubated with the probe at different concentrations for 24 h. The cell viability was measured by the MTT assay, and the data are reported as the percentage relative to the untreated cells.

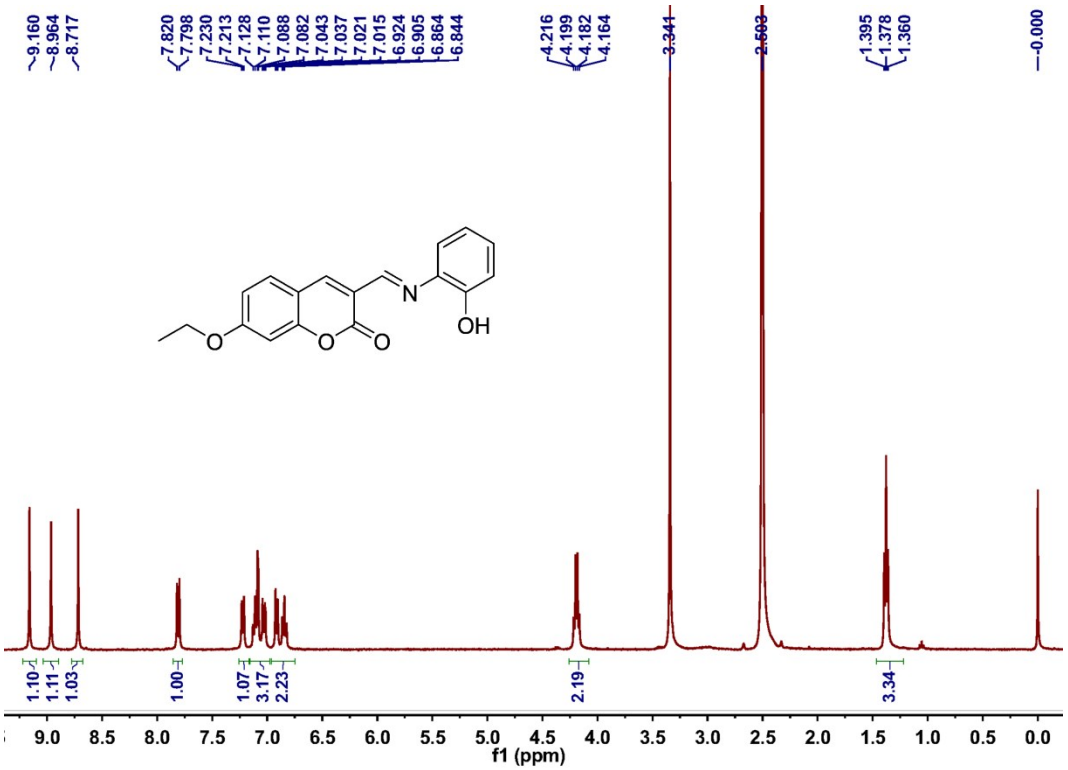

Figure S22. [1] H NMR spectra of probe **1a**.

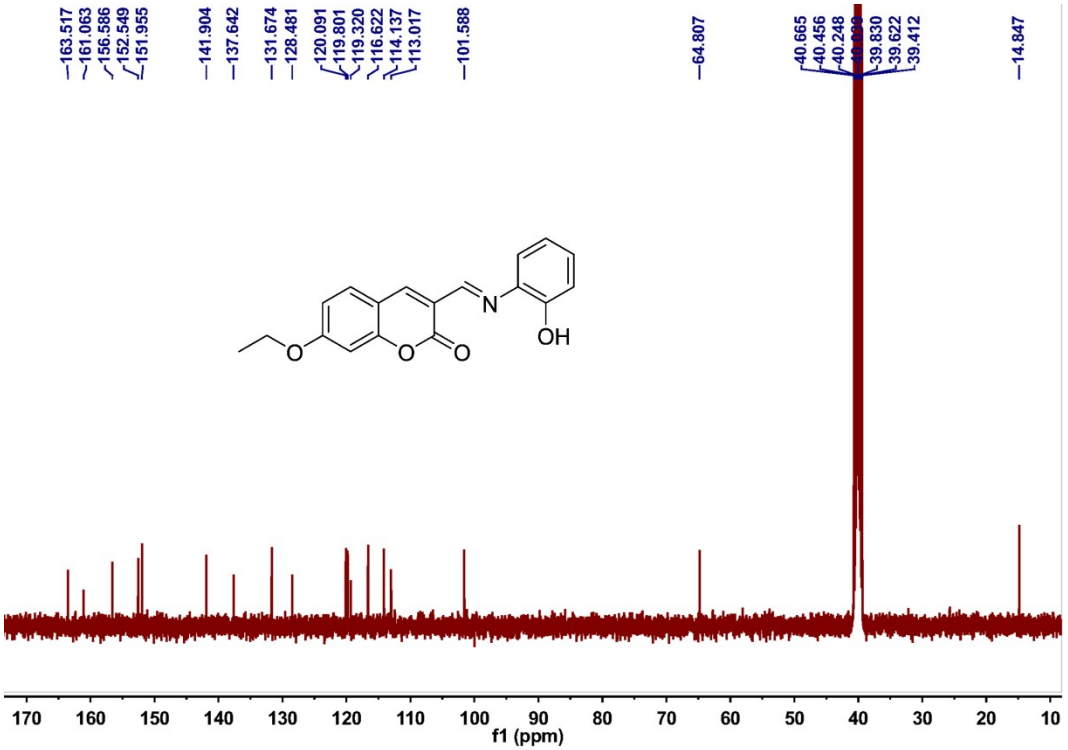

Figure S23. [13] C NMR spectra of probe **1a**.

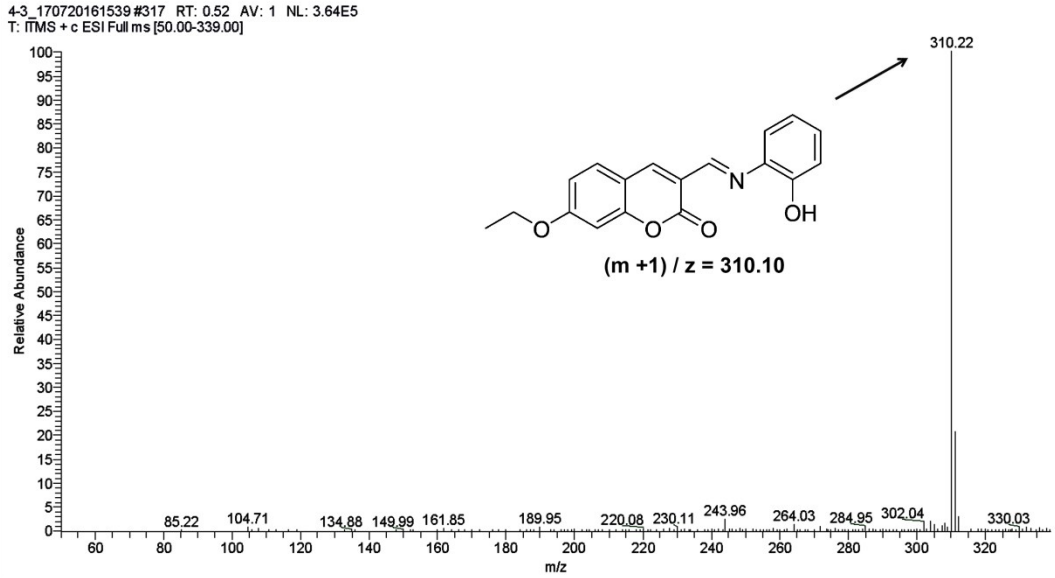

Figure S24. The ESI-Ms spectra of probe **1a**.

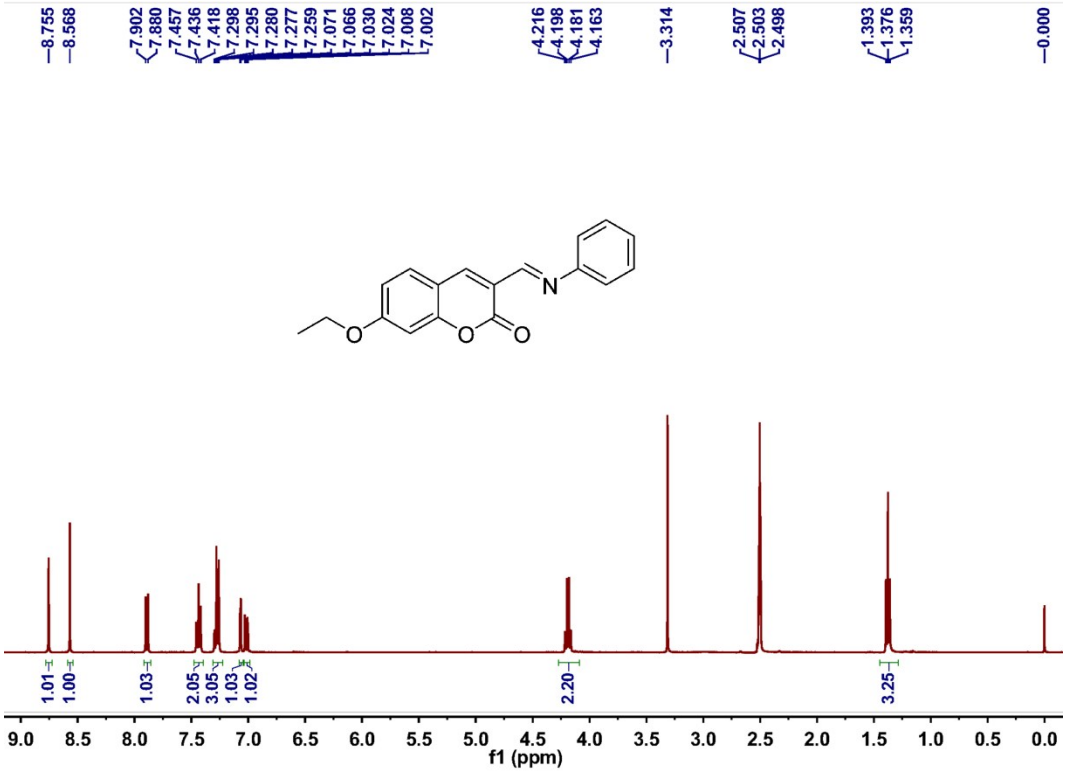

Figure S25. [1] H NMR spectra of compound **1b**.

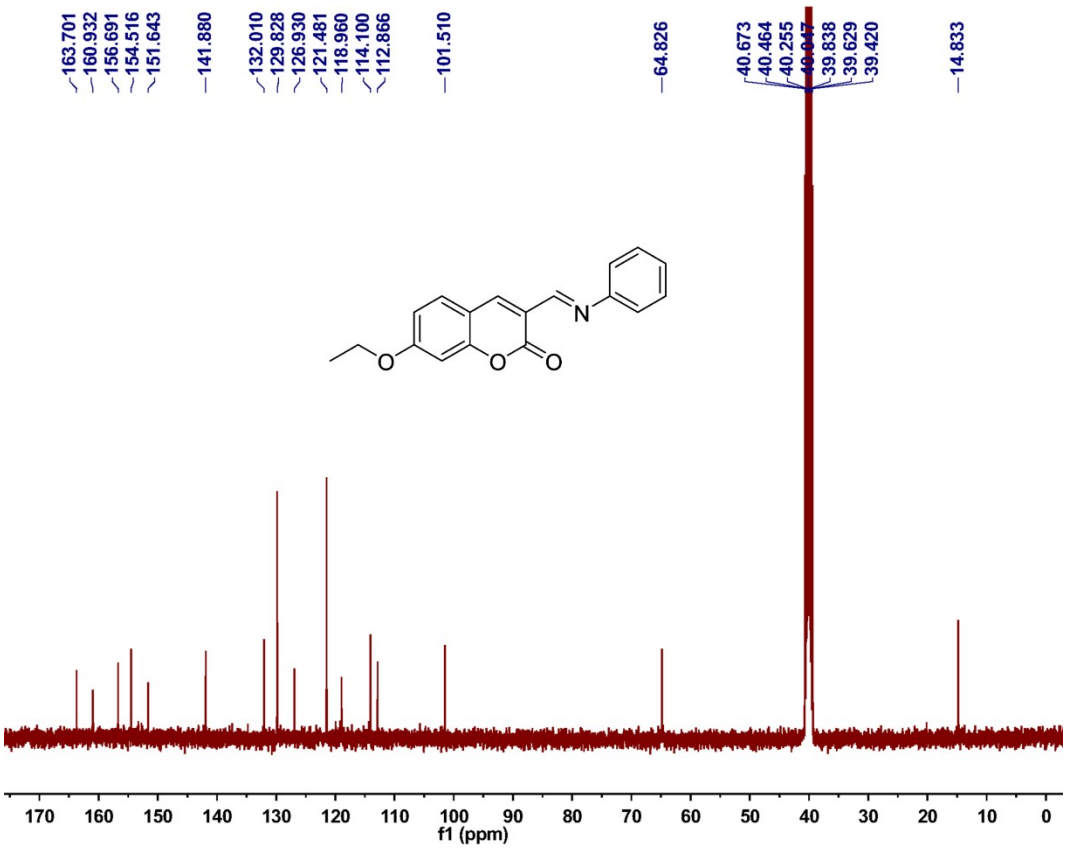

Figure S26. ^{13}C NMR spectra of compound **1b**.

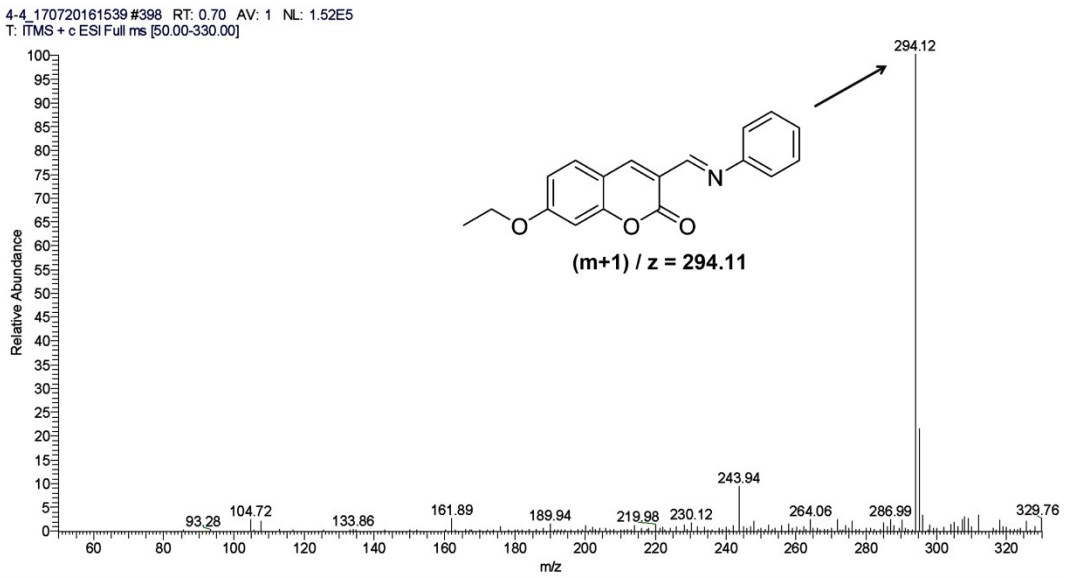

Figure S27. The ESI-Ms spectra of compound **1b**.

References

1. J. N. Demas and G. A. Crosby, *J. Phys. Chem.*, 1971, **75**, 991.
2. A. Ajayaghosh, P. Carol and S. Sreejith, *J. Am. Chem. Soc.*, 2005, **127**, 14962.
3. S. Fery-Forgues and D. Lavabre, *J. Chem. Educ.*, 1999, **76**, 1260.
4. C. A. Parker and W. T. Rees, *Analyst*, 1960, **85**, 587.
5. A. Caballero, R. Martinez, V. Lloveras, I. Ratera, J. Vidal-Gancedo, K. Wurst, A. Tarraga, P. Molina and J. Veciana, *J. Am. Chem. Soc.*, 2005, **127**, 15666.
6. B. Chandra, S. P. Mahanta, N. N. Pati, S. Baskaran, R. K. Kanaparthi, C. Sivasankar and P. K. Panda, *Org. Lett.*, 2013, **15**, 306.
7. W. D. Chen, W. T. Gong, Z. Q. Ye, Y. Lin and G. L. Ning, *Dalton Trans.*, 2013, **42**, 10093.
8. W. Lin, L. Long and W. Tan, *Chem. Commun.*, 2010, **46**, 1503.
9. M. Shortreed, R. Kopelman, M. Kuhn and B. Hoyland, *Anal. Chem.*, 1996, **68**, 1414.
10. M. J. Frisch, G. W. Trucks, H. B. Schlegel, G. E. Scuseria, M. A. Robb, J. R. Cheeseman, G. Scalmani, V. Barone, B. Mennucci, G. A. Petersson, H. Nakatsuji, M. Caricato, X. Li, H. P. Hratchian, A. F. Izmaylov, J. Bloino, G. Zheng, J. L. Sonnenberg, M. Hada, M. Ehara, K. Toyota, R. Fukuda, J. Hasegawa, M. Ishida, T. Nakajima, Y. Honda, O. Kitao, H. Nakai, T. Vreven, J. A. Montgomery, Jr., J. E. Peralta, F. Ogliaro, M. Bearpark, J. J. Heyd, E. Brothers, K. N. Kudin, V. N. Staroverov, T. Keith, R. Kobayashi, J. Normand, K. Raghavachari, A. Rendell, J. C. Burant, S. S. Iyengar, J. Tomasi, M. Cossi, N. Rega, J. M. Millam, M. Klene, J. E. Knox, J. B. Cross, V. Bakken, C. Adamo, J. Jaramillo, R. Gomperts, R. E. Stratmann, O. Yazyev, A. J. Austin, R. Cammi, C. Pomelli, J. W. Ochterski, R. L. Martin, K. Morokuma, V. G. Zakrzewski, G. A. Voth, P. Salvador, J. J. Dannenberg, S. Dapprich, A. D. Daniels, O. Farkas, J. B. Foresman, J. V. Ortiz, J. Cioslowski and D. J. Fox, Gaussian 09, Revision D.01 ed., Gaussian, Inc., Wallingford CT, 2013.